Romanian Reports in Physics **71**, 509 (2019)

ELECTRICAL CAPACITORS BASED ON MAGNETORHEOLOGICAL ELASTOMERS: EFFECTS OF THE STATIC AND PULSATING MAGNETIC FIELD ON ELECTRICAL PROPERTIES

L. M. CÎRȚÎNĂ[1, *], I. BICA[2], L. CHIRIGIU [3], D. CÎRȚÎNĂ [1, **]

[1] "Constantin Brâncuşi" University of Târgu Jiu, B-dul Republicii 1, Targu Jiu 210135, Romania
E-mail: [*] *cirtinaliviu@gmail.com* (corresponding author), [**] *danielacirtina@gmail.com*
[2] West University of Timisoara, B-dul V. Parvan 4, Timişoara 300233, Romania,
E-mail: *ioan.bica@e-uvt.ro* (corresponding author)
[3] University of Medicine and Pharmacy of Craiova, Str. Petru Rareş 2, Craiova 200349, Romania
E-mail: *liviuchirigiu@yahoo.com*

Received July 26, 2019

Abstract. Magnetorheological elastomers (MRE) based on iron microparticles and silicone rubber are used as dielectric materials for fabrication of electrical capacitors. We show that the electrical properties of the capacitors are sensibly influenced by external magnetic and electric fields. We present and describe the experimental setup used for preparation of MRE and capacitors. The physical mechanisms leading to the observed effects are explained by using the model of dipolar approximation.

Key words: magnetorheological elastomer, electrical capacitors, magnetic field, iron microparticles, silicone rubber.

1. INTRODUCTION

Magnetorheological materials (MRMs) is a class of smart materials whose physical characteristics can be changed in a few moments since the application of an external magnetic field [1–80]. The main types of materials belonging to MRMs, and which have important technical, industrial and bio-medical applications are magnetorheological suspensions (MRSs) and magnetorheological elastomers (MREs).

MRSs are generally obtained by thermal decomposition of $Fe_2(CO)_9$ particles in silicone oil [1], by a sol-gel process [66], or by manufacturing multilayer particles [49]. The later method has the advantage that it can emphasize the influence of the technological regime on their physical properties [52, 68]. Thus the obtained MRSs are widely used for fabrication of vibration absorbers [2], clutches [3], in measurement of mechanical deformation [4, 10, 17, 34, 53, 62, 78], as components for magnetic field sensors [5, 8, 10, 13, 20, 23, 26, 29, 30, 47, 48], etc. In addition, the drastic change of the rheological properties in an external magnetic field [10, 15, 50, 52, 55, 58, 59, 67, 75, 78] makes it possible to use MRMs for manufacturing of tunable couplings between active and resistive shafts [53, 59, 60, 62, 64, 71].

Generally, the physical properties of MRMs, such as electrical conductivity or thermal conductibility are changed due to a decrease of distances between the magnetic dipoles from the liquid or visco-elastic matrix. This behaviour can be induced in MRMs by using carbonyl iron and silicone oil as a matrix [4], by using graphite and γ-Fe_2O_3 microparticles as additives [5, 15] and/or by changing the amount of carbonyl iron [6–12]. In particular, when placed in a magnetic field, the electrical properties of MRMs are sensibly changed [4, 5, 7–9, 13, 15, 19, 43, 47], and this can be used for manufacturing of low-cost passive and active elements of electrical circuits with high performances [20, 23, 26, 30, 33, 36].

However, environmental friendly MRMs suitable for bio-medical applications have been obtained only relatively recently in Ref. [13], where the silicone oil matrix has been replaced with bee honey. For materials based on these MRMs it has been shown that the electrical and magnetodielectric properties can be induced by an external magnetic field [13, 14]. In addition, when the MRMs used are also stable in time, composites based on natural polymer fabrics can be fabricated [15, 16] thus leading to the possibility to manufacture magnetically active fabrics and tissues with outstanding electric and dielectric properties [14, 80].

MREs is a type of MRMs in which the magnetisable phase is in the form of ferro-ferri/magnetic nano-microparticles, and is dispersed in an elastic and/or a viscoelastic matrix [1–13]. The electroconductive, magnetodielectric and visco-elastic properties of the MREs are influenced by the magnetic field applied, the hydrostatic pressure and the additives used [17–37, 44–79]. Changes in their physical properties take place immediately after the magnetic field is applied, due to a reordering the magnetisable phase. The structural properties of the magnetisable phase are generally monitored using small-angle neutron scattering (SANS), atomic force microscopy (AFM) or computed tomography (CT) [38–41], which allows to obtain the type and magnitude of the interactions between the microparticles and the elastic matrix and respectively the roughness and fractal properties of the surfaces and aggregates inside MRE [42, 43]. Therefore, understanding these correlations, allows us to optimally design MREs with pre-established electrical properties needed for manufacturing magnetic field or mechanical deformation sensors [20–24, 26, 34, 78, 79].

In this paper we continue this research direction and present a method for manufacturing of a new class of MRE based on iron microparticles and silicone rubber, as well as the procedure of fabricating an electrical capacitor (FC) having MRE as dielectric material with very good electrical properties. We present and describe the installation for testing the FC in static and pulsating magnetic field, and in a static magnetic field superimposed on a medium frequency electrical field. We show that the equivalent electrical capacity and the equivalent electrical resistance of the FC are sensibly influenced by the magnetic field intensity and by the electric field frequency. We explain qualitatively the observed effects by using the model of dipolar approximation.

2. MATERIALS AND METHODS

The materials used for the manufacturing the FC are: iron microparticles (μFe) from Merck, with an average diameter of d = 10 μm and with density, ρ = 7.89 kg/m^3, liquid silicone rubber (SR), type RTV 3325 with viscosity 250 mPa · s at t = 25°C and catalyst type Rhodorsil Cata 6H, from Bluestar Silicone to which is added a simple plated wiring, type LAM75X100D1 from Adelaida Impex S.R.L.

The main steps in fabricating the FC are:

1. A volume of 3.0 cm^3 of iron powder is homogeneized at $t \approx 120$°C with 1.5 cm^3 of silicone rubber for about 240 s, until the temperature of the mixture becomes equal to that of the ambient. At the end of this procedure a volume of 0.5 cm^3 of catalyst is added, and the homogenization is continued for an additional 300 s, untill a dark liquid suspension is obtained, hereinafter called MRE.
2. Two wired plates are cut at dimensions 30 mm × 30 mm.
3. On each of the copper-coated side of the plates is deposited a layer of MRE which is then pressed against each other, until the distance between the plates is l = 0.22 mm. The polymerization of MRE lasts 24 hours, after which a membrane based on magnetorheological elastomer is obtained, as shown in Fig. 1. At the end of this process, an electrical connection is glued on each copper coated side (Fig. 1). Finally, the electrical capacitor FC having MRE as dielectric material is obtained (Fig. 1).

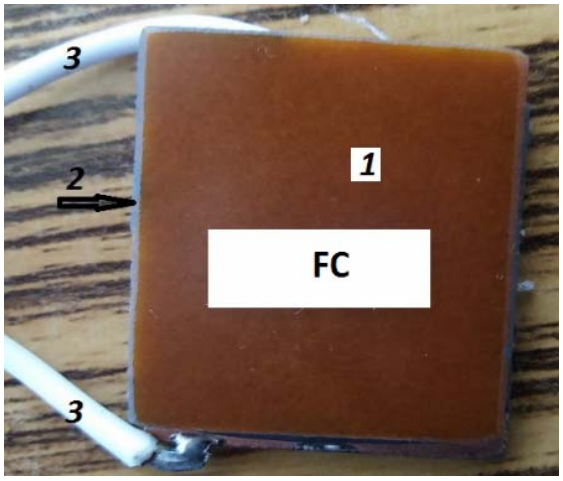

Fig. 1 – Electrical capacitor (FC) with MRE as dielectric material:
1 – wired plates, 2 – MRE membrane and 3 – electrical conductor.

The experimental setup used for magnetical characterization and for investigating the response of FC to external magnetic and electrical excitations is

shown in Fig. 2. It consists from an electromagnet with coil resistance 5.8 Ω and inductance 21 mH connected to a CPX 400D source of continuous current (not shown in Fig. 2), a DX-102 Gaussmeter with Hall probe, an RLC 8846A bridge connected to a computing unit or to the E7-20 impedancemeter, and respectively the capacitor FC, which is fixed between the N and S poles of the electromagnet.

Between the N and S poles of the electromagnetic flux density, $\vec{B}$, is fixed from the intensity of the electric current charged by the power supply. Magnetic flux density monitoring is performed with the DX-102 gaussmeter, from Dexing Magnet. By using the impedancemeter E7-20 from MNIPI, the capacity C_p, resistance R_p, impedance Z, and the phase shift φ between the dielectric polarization vector and the electric field intensity vector are measured for fixed values of the magnetic flux density, superimposed on a sinusoidal electric field of frequency up to f = 1000 kHz. R_p and C_p are measured in a static, and respectively in a pulsating magnetic field at time intervals of 1 s, with an accuracy of ±4%. The RLC bridge measures electrical resistances from 10 Ω to 1000 MΩ and capacities from 1 nF to 0.1 F. The data are recorded by a computing unit, equipped with a pre-installed software, corresponding to the RS232 interface. The pulsating magnetic field is a step-like type, with amplitudes of 100, 200, 300 and 400 mT. The pulse repetition period is fixed at an interval of 60 s.

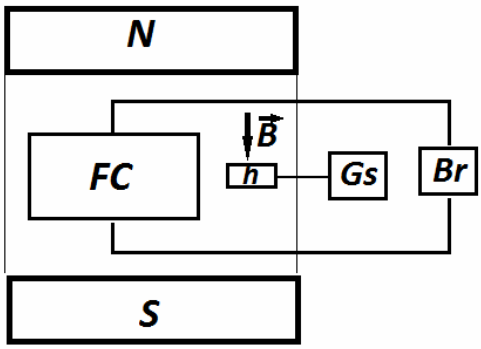

Fig. 2 – Experimental setup (overall configuration): N and S – magnetic poles of the electromagnet, Br – RLC bridge/impedancemeter, FC – electrical capacitor, Gs – Gaussmeter, h – Hall probe, $\vec{B}$ – magnetic flux density vector.

3. EXPERIMENTAL RESULTS AND DISCUSSION

The obtained values of capacitance C_p, resistance R_p are presented in Fig. 3a, while the behaviour of the quality factor Q and the phase shift ϕ is presented in Fig. 3b. The data were obtained with the E7-20 impedancemeter, and show that when overlapping the alternating electric field, at frequency f = 1 kHz over the static

magnetic field, the values of C_p and Q increase with the increase of magnetic flux density B. However, the electrical resistance R_p and the phase shift, decrease with increasing the values of B. Note that the phase shift between the dielectric polarization vector and electric field intensity vector is found between –88° at 0 mT and 70° at 440 mT, and therefore FC behaves as a real electrical capacitor. The equivalent electrical scheme of FC consists from an ideal electrical capacitor connected in parallel with an ideal resistor.

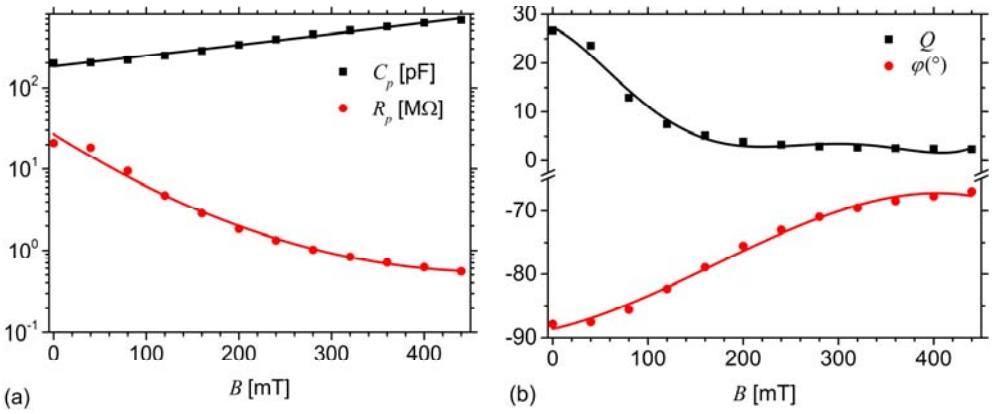

Fig. 3 – a) Capacitance C_p and resistance R_p; b) Quality factor Q and phase shift ϕ, as a function of magnetic flux density B.

By using the same impedancemeter, the capacitance C_p and the quality factor Q are measured in an alternating electric field with frequencies from 1 kHz up to 1000 MHz, at fixed values of magnetic flux density B. The obtained results are presented in Fig. 4a and respectively Fig. 4b. For a fixed value of B, C_p decreases monotonically with f, while for a fixed value of f, C_p increases with B. However, Q increases with f at fixed B, and it decreases with B at fixed f.

In order to explain qualitatively the observed effects, we consider that for the equivalent electrical capacitor, the capacitance can be approximated by:

$$C_p = \frac{\varepsilon_0 \varepsilon_r' L^2}{l}, \tag{1}$$

where ε_0 is vacuum dielectric constant, ε_r' is the relative dielectric permittivity, L is the length, and l is the thickness of the dielectric between the plates of the capacitor. By using numerical values $\varepsilon_0 = 8.85 \times 10^{-12}$ F/m, $L = 3 \times 10^{-2}$ m and $l = 22 \times 10^{-5}$ m (see Section 2) in Eq. (1), one obtains:

$$\varepsilon_r' \approx 0.028 \times C_p[\text{pF}]. \tag{2}$$

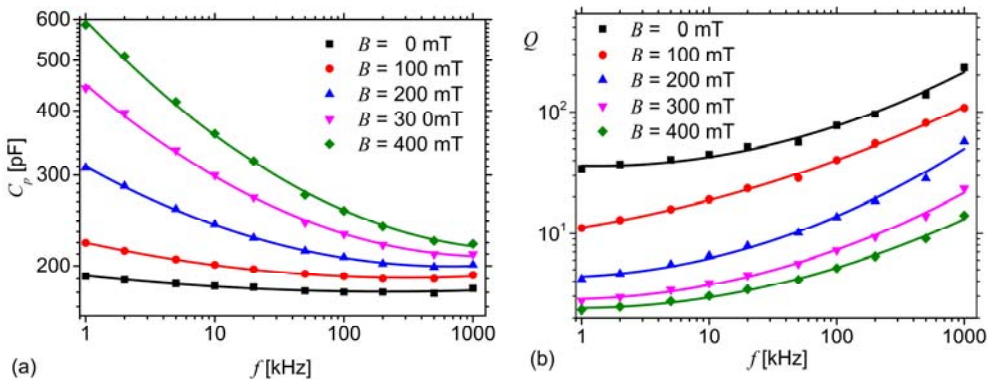

Fig. 4 – a) Capacitance C_p; b) quality factor Q, as a function of electric field frequency f for fixed values of magnetic field density B.

By introducing the capacitance $C_p = C_p(f)_B$ from Fig. 4a in Eq. (2), one obtains the variation of relative dielectric permittivity with the frequency f, for fixed values of magnetic flux density B, as: $\varepsilon_r' = \varepsilon_r'(f)_B$. The results are presented in Fig. 5a, which shows that ε_r' decreases with increasing f, at fixed B, and it increases with B at fixed f. This increase takes place as a result of the reordering of iron microparticles inside the silicone rubber matrix [14–17, 22]. Dielectric losses occur in the dielectric between the plates of the FC capacitor, as the phase shift between the polarization vector and the alternating electric field (see Fig. 3b) is $\phi < 90°$.

It is well known that between the quality factor Q and the dielectric loss tangent tan δ, the following relationship holds [81]:

$$\tan\delta = Q^{-1}. \tag{3}$$

By introducing the functions $Q = Q(f)_B$ from Fig. 4b in Eq. (3) one obtains in Fig. 5b the variation of dielectric loss tangent tanδ with frequency f, for fixed values of magnetic flux density B. The results show that the dielectric loss tangent in the FC can be controlled by the applied magnetic field, for fixed values of the electric field frequency. Also, note that the dielectric loss tangent increases with B for fixed values of f.

Variation of the resistance R_p and capacitance C_p with time t, for fixe values of magnetic flux density is presented in Fig. 6, which shows that R_p and C_p have a quasi-linear behavior. During measurements, FC has finite values of the electrical capacitance in the absence of a magnetic field. However, in the case of the equivalent electrical resistor, significantly different values of the resistance R_p are

obtained for $B > 230$ mT. Note that R_p and C_p increases and respectively decreases with magnetic flux density B.

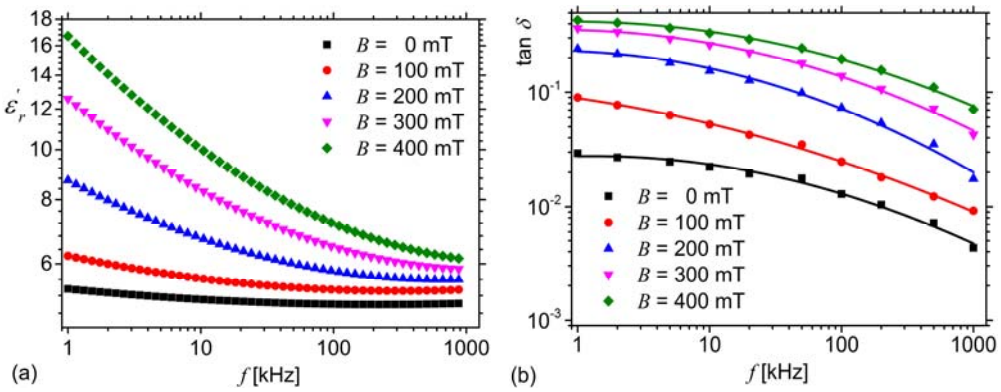

Fig. 5 – a) The relative dielectric permittivity ε_r' ; b) Dielectric loss tangent tan δ, as a function of electric field frequency f for fixed values of magnetic field density B.

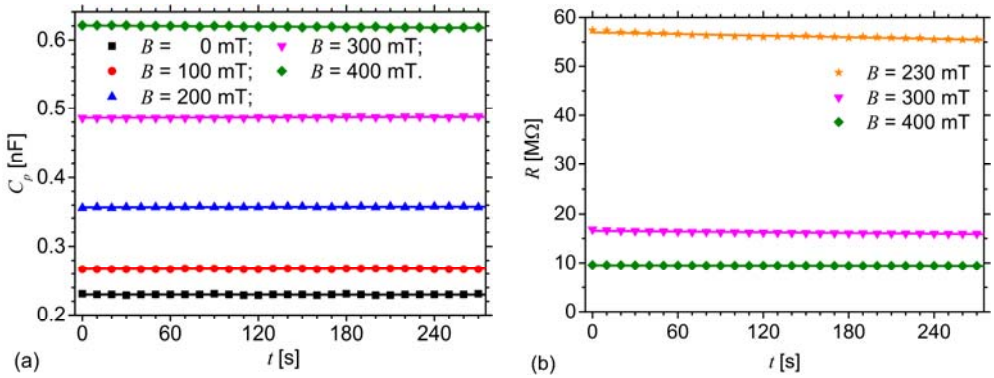

Fig. 6 – Equivalent electrical: a) capacitance C_p; b) resistance R_p as a function of time t for fixed values of magnetic field density B.

In the case of step-like pulsating magnetic field, the variation of the corresponding capacitance C_p and resistance R_p with time t is presented in Fig. 7, which shows that when a pulsating magnetic field is applied the dielectric and electric functions (Fig. 7a and respectively Fig. 7b) are characterized by transitory processes. They arise due to the modification of MRE viscosity in magnetic field [80].

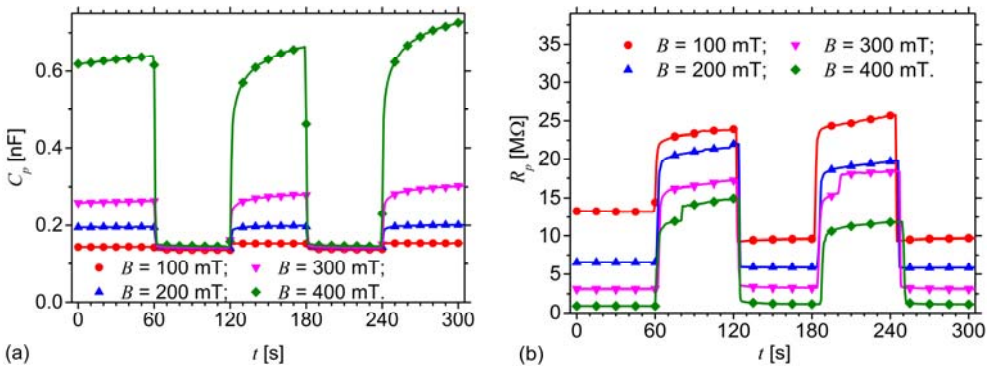

Fig. 7 – Equivalent electrical: a) capacitance C_p; b) resistance R_p as a function of time t for fixed values of magnetic field density B.

The model of FC in magnetic field is shown in Fig. 8, and it assumes that the magnetic dipoles inside the viscoelastic matrix are identical and form parallel chains of aggregates.

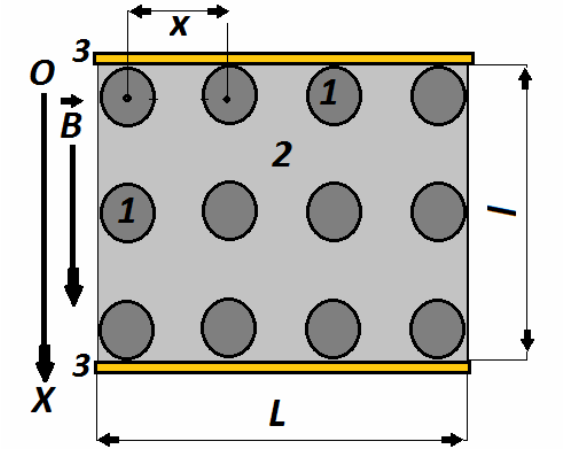

Fig. 8 – Electrical capacitor FC in magnetic field (model): 1 – magnetic dipole, 2 – viscoelastic matrix, 3 – copper electrodes, $\vec{B}$ – magnetic flux density vector, L – length of FC, l – thickness of FC, x – distance between the mass centers of magnetic dipoles, OX – coordinate axis.

At a given moment t, after the magnetic field is applied, the distance between the mass centers of the dipoles is [12–17]:

$$x = \frac{d}{\sqrt[3]{\Phi_{Fe}}}\left(1 - \frac{1.25\sqrt[3]{\Phi_{Fe}}B^2}{\mu_0\eta}t\right), \tag{4}$$

where d and Φ_{Fe} are the diameter and respectively, the volume fraction of iron microparticles, B is the magnetic flux density, μ_0 is the magnetic constant of vacuum, and η is the apparent viscosity of MRE.

From an electrical point of view, two identical and neighboring dipoles form a microcapacitor with capacitance C_{x1}, as well as a linear micro resistor with resistance R_{x1}, whose expressions are given by:

$$C_{x1} = \frac{\pi\varepsilon_0\varepsilon_r d^2}{4x}, \quad \text{and} \quad R_{x1} = \frac{4x}{\pi\sigma d^2}, \quad \text{for} \quad B \neq 0 \quad \text{and} \quad t > 0, \tag{5}$$

where x is the distance between center of masses of magnetic dipoles, σ is the electrical conductivity, ε_0 is the dielectric constant of vacuum, and ε_r is the relative dielectric permittivity.

A chain of magnetic dipoles with capacitance C_x and resistance R_x can be approximated by:

$$C_x = \frac{N}{N_1} = \frac{\pi\varepsilon_0\varepsilon_r d^3}{4lx} \quad \text{and} \quad R_x = N_1 R_{x1} = \frac{4lx}{\pi\sigma d^3}, \tag{6}$$

where $N_1 \gg 1$ is the number of magnetic dipoles forming the chain. The number of chains with magnetic dipoles can be obtained from:

$$N_2 = \frac{N}{N_1} = \frac{\Phi_{Fe} V}{V_p} = \frac{3D^2\Phi_{Fe}}{d^2}, \tag{7}$$

where N and V are the number of magnetic dipoles and respectively the volume of MRE, and V_p is the volume of a single magnetic dipole. Therefore, by using Eqs. (4–6) the electrical capacitance C_p and resistance R_p of FC can be written as:

$$C_p = N_2 C_x = \frac{3\pi\varepsilon_0\varepsilon_r D^2\Phi_{Fe}}{8l\left(1 - \frac{1.25\sqrt[3]{\Phi_{Fe}}}{\mu_0\eta} B^2 t\right)^{\frac{1}{5}}} = C_0\left(1 - \frac{1.25\sqrt[3]{\Phi_{Fe}}}{\mu_0\eta} B^2 t\right)^{-0.2}, \tag{8}$$

and respectively:

$$R_p = \frac{R_x}{N_2} = \frac{8l}{3\pi\sigma D^2\Phi_{Fe}}\left(1 - \frac{1.25\sqrt[3]{\Phi_{Fe}}}{\mu_0\eta} B^2 t\right)^{\frac{1}{5}}, \tag{9}$$

where:

$$C_{p0} = \frac{3\pi\varepsilon_0\varepsilon_r D^2 \Phi_{Fe}}{8l}, \tag{10}$$

is the equivalent electrical capacitance of FC at $B = 0$. We can observe from Eq. (8) that C_p has a linear dependence with t, in agreement with the results shown in Fig. 6a. Also, R_p sensibly decrease with increasing B, in aggrement with the experimental results shown in Fig. 6b.

The apparent viscosity is obtained from Eq. (8), according to:

$$\eta = \frac{1.25\sqrt[3]{\Phi_{Fe}}B^2 t}{\mu_0\left[1-\left(\frac{C_{p0}}{C_p}\right)^5\right]} \tag{11}$$

By using numerical values $\Phi_{Fe} = 60\%$ vol., $t = 1$s and $\mu_0 = 12.56 \times 10^{-7}$ H/m in Eq. (11) one obtains:

$$\eta = \frac{0.8394 \cdot B^2[\mathrm{mT}]t[\mathrm{s}]}{1-\left(\frac{C_{p0}}{C_p}\right)^5} \tag{12}$$

By introducing the functions $C_p = C_p(t)_B$ from Fig. 6a and Fig. 7a, one obtains in Fig. 9a and respectively Fig. 9b the variation of apparent viscosity η of MRE with time t for fixed values of magnetic flux density B, as shown. In a constant magnetic field, η increases with increasing B, and is quasi-constant for the period when the magnetic field is applied. However, when a pulsating magnetic field is applied (Fig. 9b), during the period when the magnetic field is applied, one can observe variations of η, with amplitudes which exceeds the values of η in continuous regime (Fig. 9a). The observed effects arise due to agglomeration of magnetic dipoles [45, 46] when a pulsating magnetic field is applied. When the pulsating field is switched off the aggregates are broken, and thus leading to the relaxation of apparent viscosity of MRE. This effect is seen in Fig. 9b through the absence of fluctuations for η.

4. CONCLUSIONS

A plane capacitor is manufactured having MRE as dielectric material based on silicone oil and iron microparticles, and placed between two parralel copper-coated

plates. The equvalent electrical scheme of the capacitor consists from an ideal capacitor connected in parallel to an ideal resistor.

We show that in the presence of an external magnetic field superimposed on a medium frequency electric field, both the equivalent capacitance and resistance depend on the values of the magnetic flux density as well as on the electric field frequency. We also show that in a pulsating magnetic field, the equivalent electrical capacitance and resistance are changed in accordance to the period for which the magnetic field is applied. These changes arise due to formation of chain-like aggregates consisting of electroconductive particles which tend to be align along the magnetic field lines.

The obtained results can be used for fabrication of magnetic field sensors with bio-medical, technical, and industrial applications.

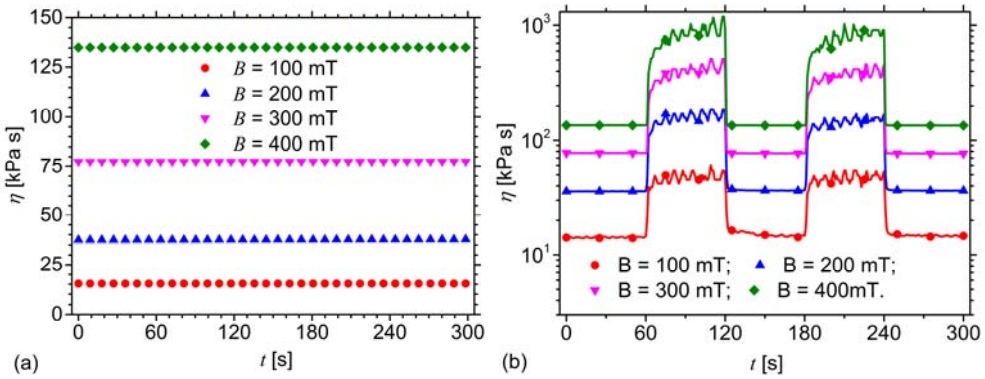

Fig. 9 – Variation of the apparent viscosity η with time t, for fixed values of magnetic flux density B: a) constant magnetic field; b) pulsating magnetic field.

Acknowledgements. The results presented in this work have been obtained in the framework of the project PN-III-P1-1.2-PCCDI-2017-0871 (CNDI-UEFISCDI) and of JINR-Romania collaboration.

REFERENCES

1. I. Bica, Mater. Sci. Eng. B. **98**, 89–93 (2003).
2. I. Bica, J. Magn. Magn. Mater. **241**, 196–200 (2003).
3. I. Bica, J. Magn. Magn. Mater. **270**, 321–326 (2004).
4. I. Bica and H. J. Choi, Int. J. Mod. Phys. *B* **22**, 5041–5064 (2008).
5. D. Gunther, D, Yu. Borin, S. Gunther and S. Odenbach, Smart Mater. Struct. **21**, 015005 (2011).
6. I. Bica, J. Ind. Eng. Chem. **13**, 299–304 (2007).
7. I. Bica, J. Ind. Eng. Chem. **12**, 806–810 (2006).
8. I. Bica, Smart Mater. Struct. **15**, N147 (2006).
9. I. Bica, Phys. B **371**, 145–148 (2006).
10. I. Bica, Y. D. Liu and H. J. Choi, J. Ind. Eng. Chem. **19**, 394–406 (2013).
11. I. Bica, M. Balasoiu, M. Bunoiu and L. Iordaconiu, Rom. Journ. Phys. **61**, 926–945 (2016).

12. I. Bica, E. M. Anitas and L. M. E. Averis, J. Ind. Eng. Chem. **27**, 334–340 (2015).
13. I. Bica and E. M. Anitas, J. Ind. Eng. Chem. **64**, 276–283 (2018).
14. I. Bica and E. M. Anitas, Mater. & Des. **155**, 317–324 (2018).
15. I. Bica and E. M. Anitas, Mater. Sci. Eng. B **236**, 125–131 (2018).
16. I. Bica and E. M. Anitas, Compos. Part B **159**, 13–19 (2019).
17. I. Bica, Y. D. Liu and H. J. Choi, Coll. Polym. Sci. **290**, 1115–1122 (2012).
18. I. Bica, J. Ind. Eng. Chem. **15,** 773–776 (2009).
19. I. Bica, Mater. Lett. 63, 2230–2232 (2009).
20. I. Bica, J. Ind. Eng. Chem. **17**, 83–89 (2011).
21. I. Bica, J. Ind. Eng. Chem, **16**, 359–363 (2010).
22. I. Bica, J. Ind. Eng. Chem. **15**, 605–609 (2009).
23. I. Bica, Mater. Sci. Eng. B **166**, 94–98 (2010).
24. I. Bica, J. Ind. Eng. Chem. **18**, 483–486 (2012).
25. I. Bica, J. Ind. Eng. Chem. **20**, 359–363 (2010).
26. I. Bica, E. M. Anitas, M. Bunoiu, B. Vatzulik and I. Juganaru, J. Ind. Eng. Chem. **20**, 3994–3999 (2014).
27. M. Bunoiu and I. Bica, J. Ind. Eng. Chem. **37**, 312–318 (2016).
28. M. Balasoiu and I. Bica, Res. Phys. **6**, 199–202 (2016).
29. I. Bica, J. Ind. Eng. Chem. **15**, 769–772 (2009).
30. I. Bica, E. M. Anitas and L. Chirigiu, J. Ind. Eng. Chem. **56**, 407–412 (2017).
31. I. Bica, M. Balasoiu and A. I. Kuklin, Sol. State Phenom. **190**, 645–648 (2012).
32. I. Bica and E. M. Anitas, Smart Mater. Struct. **26**, 105038 (2017).
33. M. Bunoiu, J. Neamtu, L. Chirigiu, M. Balasoiu, G. Pascu, I. Bica and L. M. E. Chirigiu, Appl. Surf. Sci. **424**, 282–289 (2017).
34. I. Bica, M. Balasoiu, M. Bunoiu, L. Iordaconiu and G. Cirtina, J. Optoel. Adv. Mater. **17**, 1379–1384 (2015).
35. M. Schumann, J. Morich, T. Kaufhold, V. Bohm, K. Zimmermann and S. Odenbach, J. Magn. Magn. Mater. **453**, 198–205 (2018).
36. A. M. Gavrilovici, E. M. Anitas, L. Chirigiu, I. Bica and M. L. Negrutiu, Adv. Polym. Technol. **2019**, 1983547 (2019).
37. I. Bica, E. M. Anitas, L. M. E. Averis, S. H. Kwon and H. J. Choi, J. Ind. Eng. Chem. **73**, 128–133 (2019).
38. M. Balasoiu, S. V. Kozhevnikov, Y. V. Nikitenko, G. E. Iacobescu, M. Bunoiu and I. Bica, J. Phys.: Conf. Ser. **848**, 012016 (2016).
39. E. M. Anitas, I. Bica, R. V. Erhan, M. Bunoiu and A. I. Kuklin, Rom. Journ. Phys. **60**, 653–657 (2015).
40. M. Balasoiu, V. T. Lebedev, D. N. Orlova, I. Bica and Y. L. Raikher, J. Phys. Conf.: Ser. **351**, 012014 (2012).
41. M. Balasoiu, V. T. Lebedev, Y. L. Raikher, I. Bica and M. Bunoiu, J. Magn. Magn. Mater. **431**, 126–129 (2017).
42. G. E. Iacobescu, M. Balasoiu and I. Bica, J. Supercond. Nov. Magn. **26**, 785–792 (2013).
43. E. M. Anitas, L. Chirigiu and I. Bica, *Studies of Electroconductive Magnetorheological Elastomers*, in: M. S. Kandelousi (Editor), *Electric Field*, IntechOpen, Croatia, 2017.
44. E. M. Anitas, Nanomaterials **9**, 648 (2019).
45. S. Melle, *Study of the dynamics in magnetorheological suspensions subject to external fields by means of optical techniques*, PhD Thesis, University of Madrid, Madrid, 1995.
46. P. Domínguez-García, Sonia Melle, J. M. Pastor, and M. A. Rubio, Phys. Rev. E **76**, 051403 (2007).
47. A. S. Semisalova, N. S. Perov, G. V. Stepanov, E. Yu. Kramarenko and A. R. Khokhlov, Soft Matter **9**, 11318–11324 (2013).
48. I. A. Belyaeva, E. Yu. Kramarenko and M. Shamonin, Polymer **127**, 119–128 (2017).
49. Yu. Z. Dong, S. H. Piao, K. Zhang and H. J. Choi, Coll. Surf. A **537**, 102–108 (2018).

50. S. H. Kwon. J. H. Lee and H. J. Choi, Materials **11**, 1040–1062 (2018).
51. G. I. Mikhasev, H. Altenbach and E. A. Korchevskaya, Compos. Struct. **113**, 186–196 (2014).
52. S. Aloui and M. Kluppel, Smart Mater. Struct. **24**, 025016 (2015).
53. S. R. Khimi and K. L. Pickering, Comps. Part B **90**, 115–125 (2016).
54. F. Guo, C. B. Du and R. P. Li, Adv. Mech. Eng. **6**, 629386 (2014).
55. K. H. Chung, U. C. Jeong and J. E. Oh, Polym. Eng. Sci **55**, 2669–2675 (2015).
56. S. Qi, H. Guo, J. Chen, J. Fu, C. Hu, M. Yu and Z. L. Wang, Nanoscale **10**, 4745–4752 (2018).
57. M. Sedlacik, M. Mrlik, V. Babayan and V. Pavlinek, Compos. Struct. **135**, 199–204 (2016).
58. L. M. Palacios-Pineda, I. A. Perales-Martínez, L. M. Lozano-Sanchez, O. Martínez-Romero, J. G. Puente-Cordova, E. Segura-Cardenas and A. Elías-Zúniga, Polymers **9**, 696 (2017).
59. B. Ju, R. Tang, D. Zhang, B. Yang, M. Yu, C. Liao, X. Yuan, L. Zhang and J. Liu, Polym. Compos. **37**, 1587–1595 (2016).
60. Z. W. Xing, M. Yu, S. S. Sun, J. Fu and W. H. Li, Smart Mater. Struct. **25**, 015026 (2016).
61. S.B. Kumbhar, S.P. Chavan and S.S. Gawade, Mech. Syst. Sign. Proc. **100**, 208–223 (2018).
62. M. A. Cantera, M. Behrooz, R. F. Gibson and F. Gordaninejad, Smart Mater. Struct. **26**, 023001 (2017).
63. H. S. Jung, S. H. Kwon, H. J. Choi, J. H. Jung and Y. G. Kim, Compos. Struct. **136**, 106–112 (2016).
64. Y. Li, J. Li, W. Li and H. Du, Smart Mater. Struct. **23**, 123001 (2014).
65. Y. H. Kim, W. J. Ahn, H. J. Choi and Y. Seo, Coll. Polym. Sci. **294**, 329–337 (2016).
66. H. S Chae, S. D. Kim, S. H. Piao and H. J. Choi, Coll. Polym. Sci. **294**, 647–655 (2016).
67. G. S. Wang, Y. Y. Ma, Y. Tong and X.F. Dong, Smart Mater. Struct. **25**, 035028 (2016).
68. Y. Chen, X. Huang, Z. Gong, C. Xu and W. Mou, Ind. Eng. Chem. Res. **56**, 183–190 (2017).
69. C. Kurniawan, A. S. Eko, P. T.A. Sihite, M. Ginting, P. Simamora, and P. Senayang, IOP Conf. Ser.: Mater. Sci. Eng. **202**, 012051 (2017).
70. T. H. Min, H. J. Choi, N. H. Kim, K. Park and C. Y. You, Coll. Surf. A **531**, 48–55 (2017).
71. D. Chen, M. Yu, M. Zhu, S. Qi and Z. Fu, Smart Mater. Struct. **25**, 115005 (2016).
72. P. Malecki, M. Krolewicz, F. Hiptmair, J. Krzak, J. Kaleta, Z. Major and J. Piglowski, Smart Mater. Struct. **25**, 105030 (2016).
73. M. Behrooz, J. Sutrisno, L. Zhang, A. Fuchs and F. Gordaninejad, Smart Mater. Struct. **24**, 035026 (2015).
74. J. S. An, S. H. Kwon, H. J. Choi, J. H. Jung and Y. G Kim, Compos. Struct. **160**, 1020–1026 (2017).
75. V. V. Sorokin, G. V. Stepanov, M. Shamonin, G. J. Monkman and E. Y. Kramarenko, Smart Mater. Struct. **26**, 035019 (2017).
76. N. A.Yunus, S. A. Mazlan, S. B. Choi, F. Imaduddin, S. A. A. Aziz and M. H. A. Khairi, Smart Mater Struct. **25**, 107001 (2016).
77. I. A. Perales-Martinez, L. M. Palacios-Pineda, L. M. Lozano-Sanchez, O. Martinez-Romero, J. G. Puente-Cordova, Polym. Test. **57**, 78–86 (2017).
78. H. Vatandoost, M. Norouzi, S. M. S. Alehashem and S. K. Smoukov, Smart Mater. Struct. **26**, 065011 (2017).
79. G. Du, X. Huang, Y. Li, Q. Ouyang and J. Wang, Smart Mater. Struct. **26**, 095024 (2017).
80. I. Bica and E. M. Anitas, J. Ind. Eng. Chem. **77**, 385–392 (2019).
81. J. Liu, *Models of electromagnetic properties of composite media*, PhD Thesis, Iowa State University, Ames, Iowa, 2012.